Acta Materialia 181 (2019) 408–422

Contents lists available at ScienceDirect

Acta Materialia

journal homepage: www.elsevier.com/locate/actamat

Full length article

The effects of ultra-fine-grained structure and cryogenic temperature on adiabatic shear localization in titanium

Zezhou Li [a], Shiteng Zhao [b], Bingfeng Wang [c], Shuang Cui [a, e], Renkun Chen [a], Ruslan Z. Valiev [d], Marc A. Meyers [a, *]

[a] University of California, San Diego, La Jolla, CA, 92093, USA
[b] University of California, Berkeley, CA, 94720, USA
[c] Central South University, Changsha, 410083, PR China
[d] Institute of Physics of Advanced Materials, Ufa State Aviation Technical University, Ufa, 450000, Russia
[e] National Renewable Energy Laboratory, Golden, CO, 80401, USA

ARTICLE INFO

Article history:
Received 14 July 2019
Received in revised form
3 September 2019
Accepted 7 September 2019
Available online 11 September 2019

Keywords:
Coarse-grained (CG) and ultrafine-grained (UFG) titanium
Dynamic response
Adiabatic shear localization at cryogenic temperatures
Nanograins

ABSTRACT

The deformation at low temperatures (173 K and 77 K) in ultrafine-grained (100 and 500 nm) titanium is investigated and its effect on adiabatic shear localization is established. In comparison with coarse-grained titanium, the strength of ultrafine-grained titanium is higher due to the classic Hall-Petch effect while the strain hardening approaches zero. Our results show that shear localization in dynamic deformation is also altered. The width of the shear band of coarse-grained titanium decreases from 30 to 18 μm (by 40%) with decreasing the initial deformation temperature to 77 K. In contrast, for 100 nm titanium, the width of shear band decreases more significantly, from 4 μm at room temperature to 1 μm (a 75% decrease) at 77 K. This difference is attributed to the combined effects of the decrease in the thermal conductivity and specific heat capacity, and the increase in thermal softening rate. These changes in the width are consistent with the predictions of the Grady and Bai-Dodd theories. Ultrafine- and nano-recrystallized grains are observed inside the bands which are dependent on initial grain size and initial deformation temperature. The dislocation evolution is evaluated for the different conditions using a Kocks-Mecking formulation; the rotational dynamic recrystallization mechanism responsible for forming the ultrafine/nanosized grains (40–250 nm) is successfully modeled incorporating the differences in initial temperature and grain size. Our results and analysis are important in enhancing the understanding of the structural evolution processes under high strain-rates and cryogenic temperatures.

1. Introduction

Titanium and its alloys have important technological applications such as biomedical implants, airframes, armor, tubing for heat exchangers, and turbines. The dynamic behavior, and especially the microstructure evolution inside adiabatic shear bands formed in coarse-grained titanium and its alloys at room temperature, have been revealed since 1980s [1,2] and studied extensively [3–6]. Over the past 30 years, the production of titanium and its alloys has matured more rapidly than perhaps any other structural material in the history of metallurgy [7,8]. Thus, it is of great significance to examine their mechanical performance in extreme conditions such as cryogenic temperatures and high strain rates. The mechanical behavior and shear localization mechanisms in coarse-grained (CG) titanium were examined by Meyers et al. [9,10]. Equiaxed ultrafine-grained (UFG) ~200 nm subgrains were observed inside the shear bands which are formed by a rotational dynamic recrystallization mechanism [11,12].

Nanostructured materials have been the subject of widespread research over the past decades [13–16]. The increased volume fraction of the intercrystalline regions (grain boundaries and triple junctions) can significantly alter their physical and mechanical properties [17,18]. It has also been observed that, as the grain size is reduced from microcrystalline to nanocrystalline, the slope of the Hall-Petch equation decreases as was predicted in 1982 by Meyers and Ashworth [19]. A variety of models such as the grain-boundary dislocation source-sink by Swygenhoven et al. [20], the thermal-activated grain boundary shearing by Conrad et al. [21], and the

* Corresponding author.
E-mail address: mameyers@eng.ucsd.edu (M.A. Meyers).

https://doi.org/10.1016/j.actamat.2019.09.011
1359-6454/

grain-boundary rotation and coalescence by Haslam et al. [22] were proposed to explain the deformation mechanisms in nanocrystalline materials.

In addition to the quasi-static mechanical response, the dynamic behavior of UFG and nanocrystalline materials, especially shear localization, has been intensively studied [23,24]. Jia and coauthors [25] studied the mechanical response of ultrafine-grained (UFG) 260 nm titanium under compression and tension; this material was prepared by equal channel angular pressing (8 passes) at 450 °C followed by cold rolling and annealing processes. In contrast to coarse-grained titanium, UFG titanium exhibits a limited strain-hardening ability due to the loss of dislocation accumulation mechanisms. At the same time, the strain-rate sensitivity was reduced due to an increase of strength. These combined effects of decrease of strain-rate sensitivity and strain hardening rate promote the occurrence of adiabatic shear localization in dynamic deformation. In addition, Jia et al. [26] reported that shear localization dominated the plastic deformation for nanocrystalline 80 nm iron under both quasi-static and dynamic compression, as strain hardening almost vanishes. Multiple shear bands nucleated, propagated in the planes with maximum shear stress and broadened their widths with the increase of compressive strain. The dynamic deformation and failure of UFG ~100 nm titanium was studied by Li et al. [27]. The work-hardening of UFG titanium disappears after a rapid strain hardening stage while its strain-rate sensitivity is found to be approximately the same as its coarse-grained (CG) counterpart. The microstructure inside the adiabatic shear band was found to consist of a mixture of elongated and equiaxed nanograins.

Ultrafine-grained (UFG) and nanocrystalline bcc iron, being prepared by powder metallurgy, might have weak interfaces which accelerate softening. The non-existence of strain hardening of nanocrystalline iron can trigger the formation of shear bands at a very low strain; thus, shear bands can be easily formed. In contrast, dislocations can still sustain the plastic deformation in ultrafine-grained titanium. Jia et al. [25] reported that apparent softening does occur under uniaxial compression in the UFG-Ti at strains of 20–24%, followed by catastrophic failure. Thus, it still exhibits very promising structural and biomedical applications with its superior strength and some ductility.

However, the combined influence of initial cryogenic deformation temperature and grain size on mechanical behavior and adiabatic shear localization of titanium is not yet understood. This has an important bearing on the underlying mechanism of microstructural evolution. Thus, this investigation mainly concerns two fundamental questions:

1. How does grain size affect the mechanical behavior of titanium under extreme conditions of high strain-rates and cryogenic temperatures?
2. How does cryogenic condition influence the adiabatic shear localization of CG and UFG titanium?

2. Experimental procedures

2.1. Mechanical testing

The Split Hopkinson (Kolsky) pressure bar was used to investigate the dynamic mechanical response of CG and UFG titanium. Cylindrical specimens, with both length and diameter of 4 mm, were deformed starting at room (293 K) and low (173 K and 77 K) temperatures. Hat-shaped specimens were used to generate high shear strains in a localized region, thus inducing forced shear localization [28]. The dimensions of hat-shaped specimens [9] used to induce shear bands were the same for each material. All the cryogenic temperature tests were performed inside an enclosed chamber (containing liquid nitrogen). The temperature inside the chamber was measured by a thermocouple after it was stable.

2.2. Microstructural characterization

Commercially pure (Grade 2) CG (~10 μm) titanium was chosen for this study, while the as-received UFG titanium rods were prepared by the severe plastic deformation (SPD) technique [7] in two slightly different sequences. The experiments were performed on Grade 4 Ti produced by Dynamet Inc. (Washington, PA, USA) in the form of hot-rolled rods with 15 mm diameter and an average grain size of ~25 μm. The chemical composition of the material, in wt.%, was 0.36% O, 0.15% Fe, 0.05% C, 0.007% N, and 0.0021% H with Ti as the balance. The rods were subjected to processing using the ECAP–Conform facility in Ufa with an angle of 120° in the ECAP abutment. The rod undergoes a total of six passes using route B_C, when the rods are rotated by 90° in the same sense between each pass, resulting in an ultrafine grain size ~100 nm [29]. In these experiments, the UFG structure was produced by means of ECAP–Conform at 473 K and then drawing at 473 K to a total accumulated strain of ~80%. The deformation process has been described with more details elsewhere [30]. Dyakonov et al. [31] examined the grain refinement mechanism of coarse-grained pure titanium under equal-channel angular pressing, and revealed that mechanical twinning was observed but the contribution of twinning to global grain refinement is relatively limited. Instead, the continuous formation of geometrically-necessary boundaries dominated the microstructural evolution. The post-annealing of severely-deformed UFG titanium was generally able to decrease the dislocation density [32]. Fig. 1(a1) shows the average grain size of the 500 nm UFG titanium. The low dislocation density inside the grains and accumulated dislocations near the grain boundaries in Fig. 1(a1) and 1(a2) indicate that the material underwent dynamic recovery and recrystallization processes during severe plastic deformation. The corresponding selected-area diffraction (SAD) pattern in Fig. 1(a3) shows the polycrystal structure. Fig. 1(b1) shows another as-received UFG titanium with average grain size 100 nm. Fig. 1(b2) shows the equiaxed configuration of grains. The high-resolution image in Fig. 1(b3) confirms its initial HCP crystal structure.

For microstructural examination, the deformed hat-shaped samples were cut parallel to the shear band. The shear bands were examined in a Phillips XL30 scanning electron microscope (SEM). A standard polishing procedure was used to prepare ∅ 3 mm transmission electron microscope (TEM) slice samples containing the shear band formed at 293 K for UFG 500 nm titanium. Focused ion beam (FIB) technique was used to accurately extract the TEM sample from inside the narrow shear bands for all the other CG and UFG titanium samples. The FIBed samples were then characterized by JEOL-2800 and Tecnai G^2 Sphera FEI transmission electron microscopes operating at 200 kV.

2.3. Thermal conductivity of UFG titanium

The van der Pauw method [33,34] was used to measure the thermal conductivity of four UFG 500 nm titanium samples at room temperature. The electronic component of the thermal conductivity (λ_e) was extracted from the measured electrical conductivity (σ_e) via the Wiedemann-Franz law:

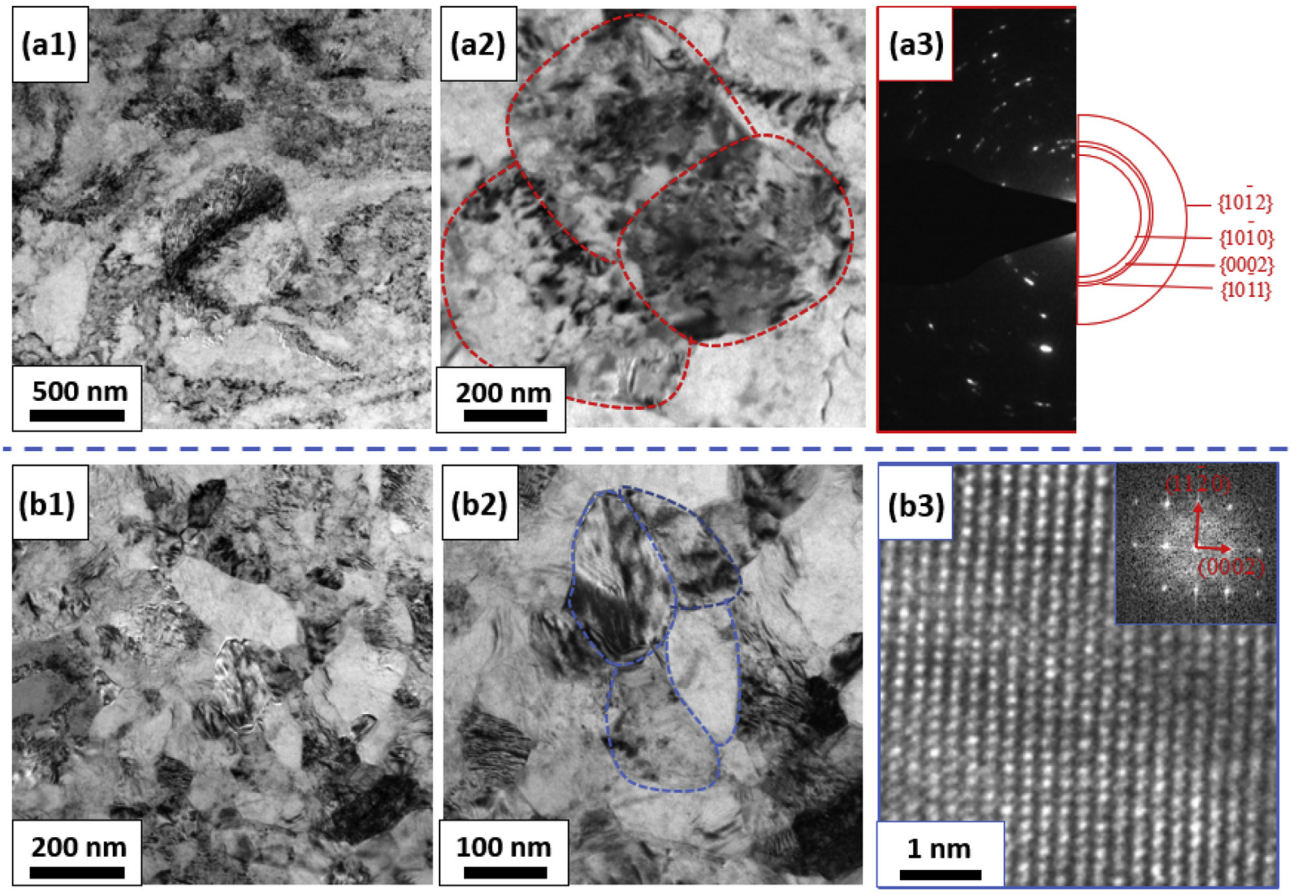

Fig. 1. (a) Transmission electron microscopy images of Ti with average grain size of 500 nm; (a2) detailed microstructure; (a3) selected area diffraction (SAD) pattern of (a1). (b) Transmission electron microscopy images of Ti with average grain size of 100 nm; (b2) detailed microstructure; (b3) high-resolution TEM image showing hcp crystal structure of Ti.

$$\frac{\lambda_e}{\sigma_e} = L_N T, \tag{1}$$

where λ_e is the electronic thermal conductivity, and $L_N = 2.44 \times 10^{-8} W \cdot \Omega \cdot K^{-2}$ is the classic Lorenz number for metals based on the Wiedemann-Franz law [35]. Here we use λ_e to represent the total thermal conductivity because it is the dominant contribution in metals at room and low temperatures [36].

3. Results and discussion

3.1. Mechanical behavior of UFG titanium

3.1.1. Microhardness

Vickers microhardness tests were performed on the bulk samples, and the values were converted to yield stresses through $\sigma_y = H_V/3$. The results in Fig. 2(a) show that the yield stress of UFG titanium increases with decreasing grain size but tends to deviate from the conventional Hall-Petch slope. Sergueeva et al. [37] summarized the microhardness of titanium with different grain sizes and found that it followed the Hall-Petch relationship down to a grain size of 10 nm. However, Meyers et al. [17] showed that the Hall-Petch slope decreases from 12.5 GPa $nm^{1/2}$ to 4.38 GPa $nm^{1/2}$ in the nano-range. The decrease in the Hall-Petch slope was mainly attributed to different deformation mechanisms gradually becoming dominant. Fig. 2(a) shows that the yield stress for UFG titanium still follows the Hall-Petch relationship [38] but that the slope decreases with decreasing grain size.

3.1.2. Mechanical response of UFG titanium at cryogenic temperatures

Fig. 2(b) shows the true stress - true strain plots of CG and UFG titanium at high strain-rates and various temperatures. It is apparent that the yield stress of both UFG and CG titanium increases with decreasing temperature and increasing strain-rate. In contrast with the clear strain hardening of CG titanium [39], the flow stress of UFG Ti is relatively flat, and no significant strain hardening is observed at either room or low temperatures. Jia et al. [40] reported a transition from strain hardening to strain softening of UFG iron as the grain size changed from ~1 μm to ~300 nm; this apparent strain softening appeared at a very low plastic strain for grain sizes below 300 nm. However, no significant strain softening was observed in UFG titanium under dynamic deformation. In addition, no ductile-to-brittle transition was observed at 77 K in dynamic deformation, indicating that the material can still exhibit significant plasticity.

Ko et al. [41] studied UFG titanium (fabricated by severe plastic deformation process) in tension, and proposed that the absence of strain hardening behavior was caused by a dynamic recovery process balancing the dislocation generation rate with the annihilation rate of trapped lattice dislocations into non-equilibrium grain boundaries. Bengus et al. [42] reported a substantial increase in the tensile yield stress (by a factor of 1.5–2) and decrease in the elongation for UFG (~300 nm) titanium, when the testing temperature decreased from 300 K to 4.2 K. Nemat-Nasser et al. [43] and Chichili et al. [44] studied the dynamic response of CG titanium over a wide range of temperatures and strain-rates. Nemat-Nasser

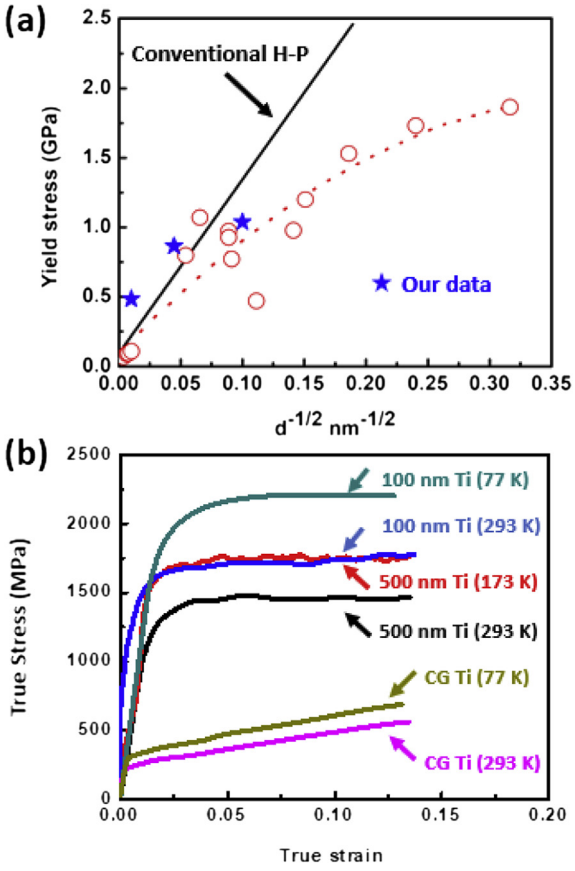

Fig. 2. (a) Hall-Petch relationship of titanium from microhardness measurements (blue stars) and comparison with literature results (red circles and line) [17]. (b) Stress-strain curves of Ti with different grain sizes at dynamic loading strain-rates ~10^3 s^{-1} [39]. (For interpretation of the references to colour in this figure legend, the reader is referred to the Web version of this article.)

et al. [43] reported that the density of twins of CG titanium increased markedly with increasing strain-rate or strain and decreasing temperature. Twin intersections occur and become more pronounced at low temperatures or high strain-rates, which can contribute to the steady work-hardening. In comparison with CG titanium, the strain hardening rate ($\frac{d\sigma}{d\varepsilon}$) of UFG titanium was significantly lower. Due to the small grain size of UFG titanium, the capacity for the accumulation of dislocations and twin boundaries significantly decreases. Hence, strain hardening of UFG titanium remains very limited and is far less than that of CG titanium.

The strain-rate sensitivity ($m = \frac{\partial \log \sigma}{\partial \log \dot{\varepsilon}}$) of titanium does not change significantly with decreasing temperature, while CG titanium deforms by mechanical twins at 77 K [43] and UFG titanium deforms mainly by dislocation slip. The activation volume for deformation can be expressed as $V = \frac{kT}{m\sigma_y}$, where k is Boltzmann's constant, T is temperature, and σ_y is the yield stress. Thus, the decrease in temperature and increase in yield stress lead to a decrease in the activation volume of dislocations. This is demonstrated by the rapid plateau of strain hardening in UFG titanium shown in Fig. 2(b).

3.2. Adiabatic shear-banding at room and cryogenic temperatures

To examine the grain size and temperature effects on shear localization in titanium, the hat-shaped samples were tested at room temperature (293K) and low temperatures (173 K and 77 K).

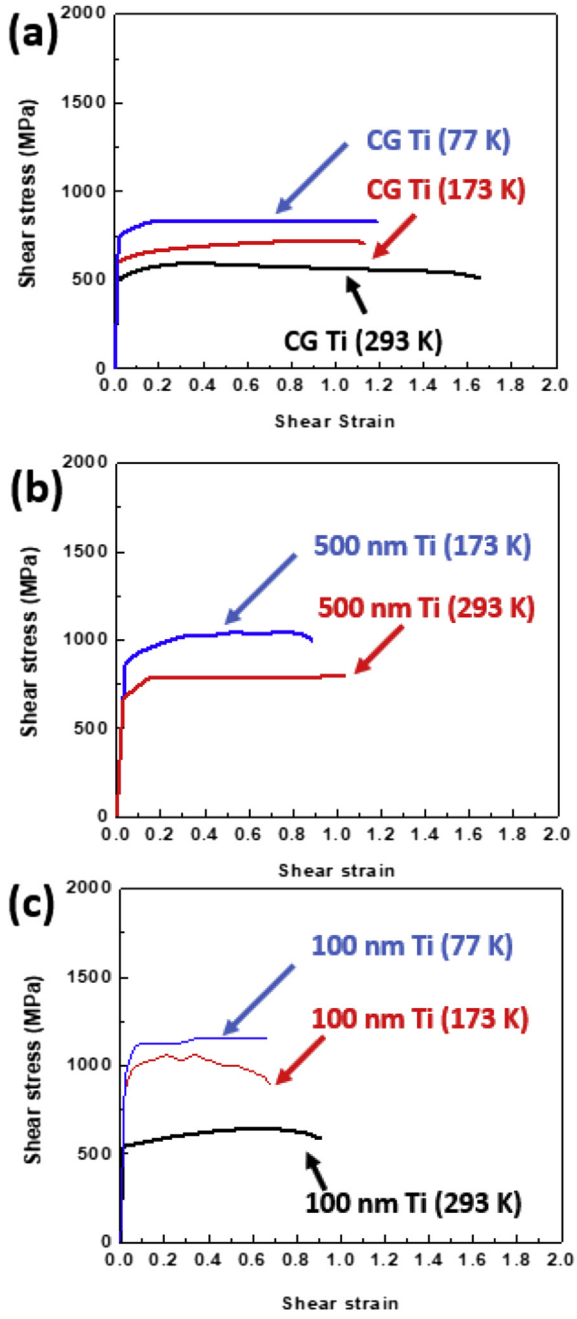

Fig. 3. (a) Shear stress vs. shear strain relationship in hat-shaped specimens of CG titanium [11]. (b) Shear stress vs. shear strain in hat-shaped specimens of UFG 500 nm titanium. (c) Shear stress vs. shear strain in hat-shaped specimens of UFG 100 nm titanium [27].

The shear stress versus shear strain curves are shown in Fig. 3 [45]. It should be noticed that the shear strain is calculated by the displacement divided by the width of shear region in the hat-shaped specimen. With increasing strain, the flow stress begins to fluctuate due to the competition between strain hardening, strain-rate hardening, and thermal softening. When the thermal softening effect becomes dominant, the stress decreases sharply and a complete adiabatic shear band (ASB) is generated. Fig. 3 indicates that the samples tested at low temperatures were loaded to higher shear stress, in comparison with the samples tested at room temperature, consistently with the mechanical behavior of titanium discussed in Section 3.1.2.

Assuming adiabatic heating, it is possible to estimate the temperature rise within the shear deformation region. Taking into account that a fraction β of the work done is converted into heat, temperature rise ΔT is [46]:

$$\Delta T = \frac{\beta}{\rho C_p}\int_{\gamma_s}^{\gamma_e} \tau d\gamma \tag{2}$$

The initial conditions are $\gamma_s = 0$, $\beta = 0.9$, $C_{p(T=273K)} = 520$J/(kg·K), $C_{P(T=173K)} = 430$ J/(kg·K), $C_{P(T=77K)} = 210$J/(kg·K), and $\rho = 4500$kg/m^3 [27]. A calculated temperature rise of at least 300 K can be reached for all of the tested samples as determined from Eqn. (2). Since the width of shear band is significantly lower than the shear region of hat-shaped specimens, the actual local shear strain in the shear band is indeed much larger than the values shown in Fig. 3. Using the in-situ infrared detector, at the onset of the load drop, Guo et al. [47] reported that severe strain localization happened first, before the temperature rises to 643-943 K for coarse-grained pure titanium.

3.2.1. Width of shear band

The widths of shear bands for CG titanium are shown in Fig. 4(a1, b1, c1). They decrease from ~30 μm at 293 K to ~18 μm at 173 K. In comparison, the shear-band width decreases from ~15 μm at 293 K in Fig. 4(a2) to ~5 μm at 173 K in Fig. 4(c2) for UFG 500 nm titanium. Shear-band bifurcation (within the red dashed lines) was observed at low temperature as shown in Fig. 4(b2). Xue et al. [48] observed this important feature of shear bands in the imploding cylinder geometry; in that case they are geometrically necessary under high strain-rate deformation. For the 500 nm titanium, the width of the shear band is slightly lower at room temperature in comparison with CG titanium. In contrast, the width decreases much more significantly at low temperatures. In addition, there is an obvious drop in the width of shear bands for UFG 100 nm titanium as shown in Fig. 4(a3,b3,c3). They decrease significantly from 4 to 1 μm as shown in Fig. 4(c3). Two theories were proposed to predict the shear-band width; they are used here to evaluate the effects of temperature and grain size. The Bai-Dodd equation [49] predicts the width, δ, of the shear bands as:

$$\delta = 2\left(\frac{\lambda T}{\tau\dot{\gamma}}\right)^{1/2} \tag{3}$$

where λ is the thermal conductivity; T, $\dot{\gamma}$, and τ are the temperature, shear strain-rate and shear stress inside the shear band. Alternatively, Grady [50,51] found that the shear-band width at minimum dissipation corresponded to a maximum shear-band growth rate. He derived the following expression for the width of shear band, incorporating the thermal softening parameter $\alpha = \frac{1}{\sigma_y}\frac{\partial\sigma}{\partial T}$ [50,51]:

$$\delta = \left(\frac{9\lambda^3}{\tau^3 C_p \alpha^2 \dot{\gamma}}\right)^{1/4} \tag{4}$$

where C_p is the specific heat capacity [9,27] and the other symbols are defined above. These two classic models predict a reduced width δ with increasing strength, strain-rate, thermal softening, specific heat capacity, and decreasing thermal conductivity. The

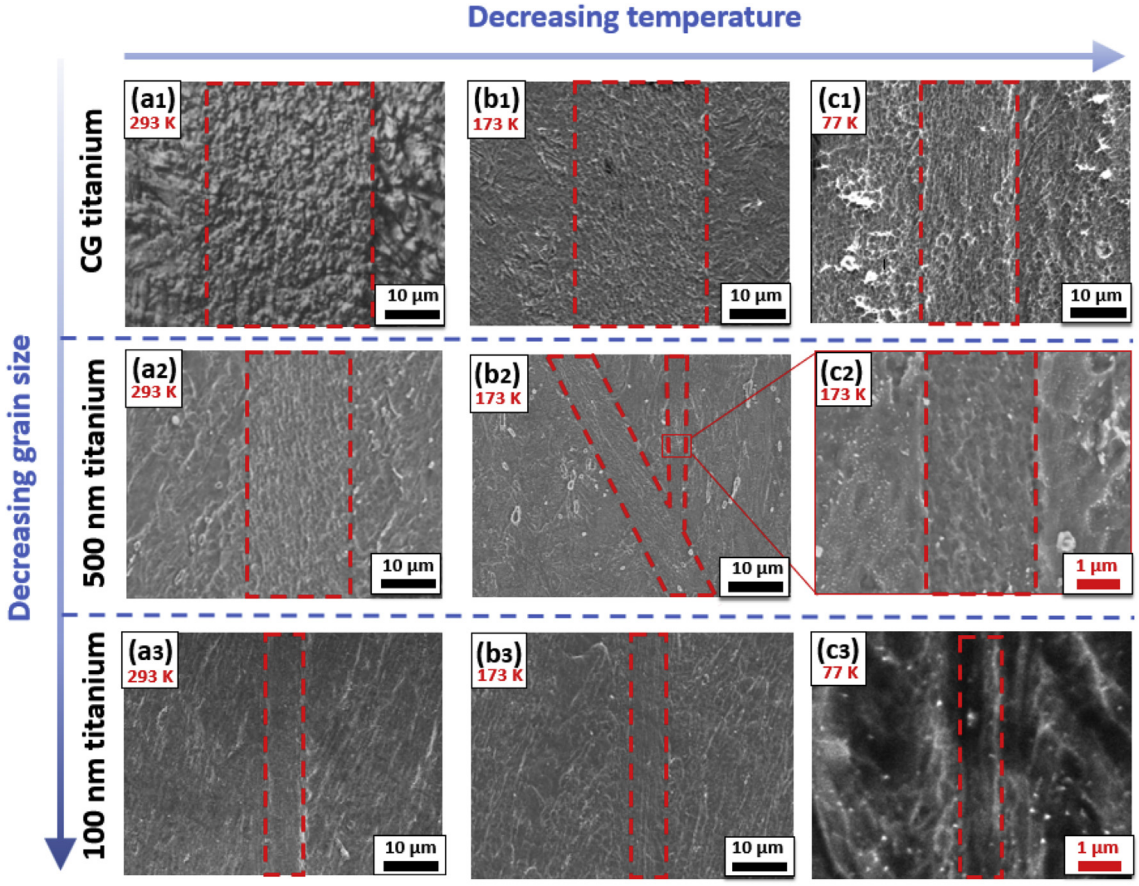

Fig. 4. SEM images showing the width of shear bands for different titanium conditions at different initial deformation temperatures.

sub-sections below show how these parameters vary for the materials under study. They are affected by grain size and temperature.

3.2.1.1. Effect of thermal conductivity. Thermal conduction in solids includes electron and phonon contributions. In general, in pure metals, the main contribution to thermal conductivity comes from electrons [36]. The measured electrical resistivity of the thick UFG 500 nm titanium disks was $0.59\pm0.01\mu\Omega$. Thus, applying the Wiedemann-Franz law represented by Eqn. (1), the electronic thermal conductivity is reduced from 22 W m^{-1} K^{-1} [9] for coarse-grained to 12.12 W m^{-1} K^{-1} (~45% reduction) for UFG Ti as shown in Fig. 5(a).

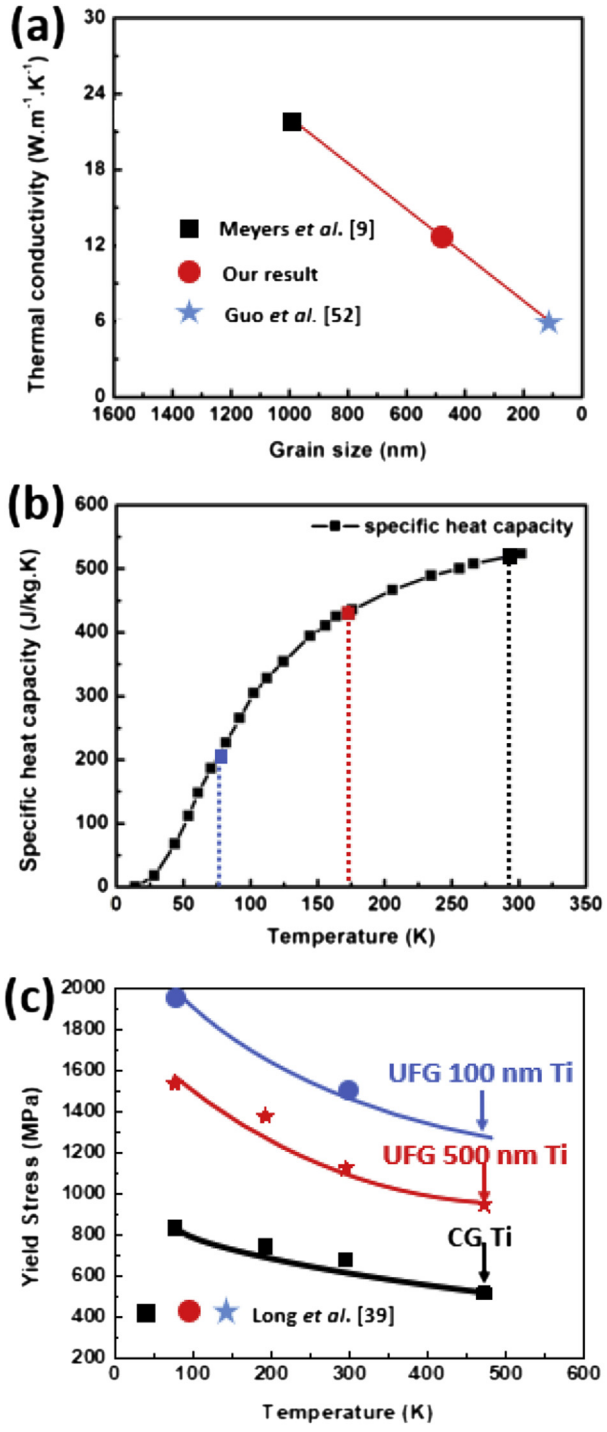

Fig. 5. (a) Effect of grain size on the thermal conductivity of titanium [9,52]. (b) Theoretical values of specific heat capacity of titanium as a function of temperature. (c) Thermal softening in CG and UFG titanium [39].

Guo et al. [52] examined the thermal conductivity of nanostructured titanium by scanning thermal microscopy that allowed it to be mapped down to the submicron scale. The analysis showed that the thermal conductivity decreased to 5.2 W m^{-1} K^{-1} for nanostructured titanium from 22 W m^{-1} K^{-1} for coarse-grained Ti. The thermal conductivity is related to the effective conduction electron density. The volume fraction of triple junctions and grain boundaries is still quite small for ultrafine-grained materials. However, the number of grain boundary barriers per volume is significantly increased with the reduction of grain size down to 100 nm. This leads to a decrease of the effective electron density, leading to the significant decrease of thermal conductivity in ultrafine-grained titanium.

3.2.1.2. Effect of heat capacity. Heat capacity of metals is contributed by lattice vibration. Debye [53] assumed that the range of frequencies of vibration available to the oscillators was the same as that available to the elastic vibrations in a continuous solid. The lower limit of the wavelengths of these vibrations was determined by the interatomic distances in the solid. He obtained the following expression for the heat capacity of solids under constant volume:

$$C_v = 9R\left(\frac{T}{\theta_D}\right)^3 \int_0^{\theta_D/T} \frac{x^4 e^{-x}}{(1-e^{-x})^2} dx \tag{5}$$

where $x = h\upsilon/kT$ (h is the Planck's constant), $R = 8.314$ J/(K·mol) and the Debye frequency is $\upsilon_D = 8.75\times10^{12}$ s^{-1}. $\theta_D = h\upsilon_D/k = 420$ K is the characteristic Debye temperature for titanium [54]. Fig. 5(b) shows that the specific heat capacity for both CG and UFG titanium decreases with decreasing temperature due to the lower population of thermally excited phonon modes [55]. Thus, $C_{T=293K} = 520$ J/(kg·K) decreases to a much lower value of $C_{T=77K} = 210$ J/(kg·K) at 77 K. The heat capacity does not change significantly when decreasing the grain size down to 100 nm, since the major contribution was due to the lattice vibration. Thus, the relatively small volume fraction of grain boundaries plays a very minor influence. The decrease of specific heat capacity will cause a more rapid increase of temperature for the same deformation energy and contribute to a narrower shear region.

3.2.1.3. Effect of thermal softening. The thermal softening parameter:

$$\alpha = -\frac{1}{\sigma_y}\left(\frac{\partial\sigma}{\partial T}\right)_{\gamma,\dot{\gamma}} \tag{6}$$

is obtained from the temperature dependence of the yield stress. To a first approximation, the strain softening of UFG 100 nm titanium ($\alpha_{UFG}\approx0.002$) is larger than that of CG Ti ($\alpha_{CG}\approx0.001$) at 77 K [56].

3.2.2. Combined effects on shear-band width

Here we discuss the three effects and apply them to the Bai-Dodd and Grady equations. First, the reduction of the thermal conductivity of nanostructured titanium at room temperature, as shown in Fig. 5(a), leads to the decrease in the width of shear band according to Eqn. (3) [49]. It was also reported that the thermal conductivity of titanium does not change significantly when decreasing the temperature to 77 K [57,58]. The lower specific heat capacity at cryogenic temperature transfers more heat under the

same input of plastic work, and low thermal conductivity provides the material a slow diffusion rate of heat to the surroundings. In addition, the increase of the thermal softening parameter contributes to the narrower width of shear band according to Eqn. (4). Also, increased thermal softening and decreased strain hardening can make UFG material more prone to shear localization, which has also been reported in UFG iron [40]. Thus, the higher thermal softening of UFG titanium at 77 K, as shown in Fig. 5(c), also contributes to the decrease in the width of shear bands.

The effects of these parameters are incorporated into the Bai-Dodd and Grady equations and plotted in Fig. 6. The decrease in the width of shear band of UFG titanium at initial cryogenic temperatures can be attributed to the decrease of thermal conductivity, the decrease of heat capacity, and the increase of thermal softening as presented in Fig. 5. Parameters in Table 1 were applied to the Bai-Dodd and Grady equations to predict width of shear bands in both CG and UFG (100 nm) titanium. The predictions of the two equations are provided in Fig. 6, together with the experimental results. The predictions of the Bai-Dodd and Grady theories use the heat capacity at room temperature. The experimental results show a more drastic dependence on strength than the predictions from the Bai-Dodd and Grady equations; for lower strength, they are close to the CG Bai-Dodd equation and for higher strength, they approach the Grady equation. The effects of a decreased thermal conductivity and increased thermal-softening are confirmed.

Hines and Vecchio [59,60] studied shear localization of shock-hardened copper [61] at initial deformation temperatures of 293 K and 77 K and similar levels of deformation. The width of shear bands did not change significantly and was in the range 200–250 μm. However, copper is FCC and exhibits a very low thermal softening component. Thus, the strengths at 293 and 77 K are not significantly different. In the current work, the width of the fully developed shear band of CG titanium dropped from 30 to ~18 μm when the initial deformation temperature was cryogenic, a 40% decrease. In contrast, the width decreases more significantly for both UFG 500 nm and 100 nm titanium at low temperature, from 4 to 1 μm, a 75% decrease. Since the temperature difference inside and outside the shear band does not have too much significance, the heat diffusion-rate effect on width of shear band is not thought to be critical. However, in Eqn. (3), the width of shear band decreases with the decrease of the thermal conductivity. In addition, from Eqn. (4), the width of shear band decreases with the increase of thermal softening parameter. One would expect that an extremely narrow shear band should form with further decreasing temperatures and increasing strain-rates [62–67].

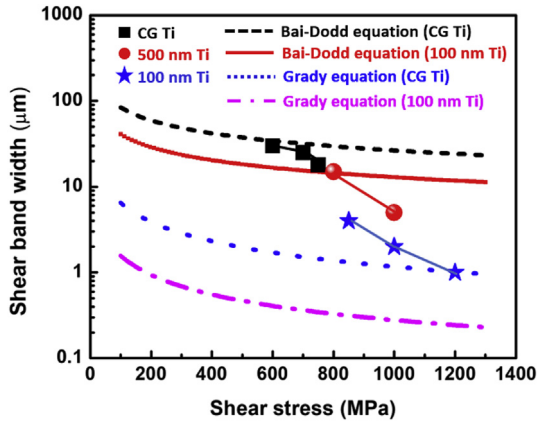

Fig. 6. Width of the shear band in pure titanium for different grain sizes and temperatures: comparison of Bai-Dodd and Grady theories with experimental results [9,49–51]. The full line represents the Bai-Dodd equation prediction applied to 100 nm titanium. The black dotted line corresponds to Bai-Dodd equation for CG Ti. Dash dotted (100 nm Ti) and dotted (GG Ti) lines correspond to Grady theory.

Table 1
Parameters for the Bai-Dodd [49] and Grady [50,51] equations.

Parameters	Values
$\lambda(CG-Ti)$	22 W m^{-1} K^{-1}
$\lambda(100nm-Ti)$	5.2 W m^{-1} K^{-1}
ρ	4500 kg/m^3
$C_{p(T=293K)}$	520 J/(kg·K)
$\dot{\gamma}$	10^5 s^{-1}
$\alpha_{100nm-Ti}$	0.002
α_{CG-Ti}	0.001
T	800 K

3.3. Microstructural evolution inside the shear bands

Fig. 7 shows TEM micrographs from the shear bands. The corresponding selected area electron diffraction (SAED) patterns for each image demonstrate the preponderance of randomly distributed recrystallized grains. The selected area electron diffraction (SAED) patterns do not suggest strong texture, with an apparent absence of concentrated intensity in the ring pattern. The shear bands contain both elongated and equiaxed grains in Fig. 7(a1), which are much smaller than the grains in the matrix. Due to dynamic recrystallization, the overall dislocation density decreases significantly inside the shear bands. Dislocations are again generated because of the continuing deformation (post recrystallization). The average grain size inside the shear band of CG titanium at 77 K is 140 nm as observed in Fig. 7(c1); this is much smaller than the average grain size of 250 nm inside the shear band formed with initial deformation at room temperature of CG titanium [9] (Fig. 7(a1)).

For UFG titanium, the average recrystallized grain size within the shear bands decreases with the lowering of the initial temperature. Fig. 7(a2) shows elongated grains breaking up into recrystallized subgrains. A higher magnification image in Fig. 7(b2) illustrates the formation of equiaxed grains. Fig. 7(c2) shows that UFG subgrains with average grain size of 120 nm were formed inside the shear band with deformation initiated at 173 K. Fig. 7(a3) shows the formation of nano-bundles during the shear deformation in UFG 100 nm titanium at 293 K. The red arrow shows a series of nano-bundles ranging from 30 nm to 80 nm. Fig. 7(b3,c3) illustrate the formation of extremely small nanograins inside the shear bands at cryogenic temperatures. No deformation twins are found inside any of shear bands, further evidence of dynamic recrystallization.

Fig. 8 shows higher magnification images of subgrains inside the shear bands. Very fine recrystallized grains are the dominant feature. Fig. 8(a1) shows that the UFG elongated dislocation cells were formed in the shear band at room temperature for CG titanium. The dark-field image of Fig. 8(b1) shows subgrains with grain size around 140 nm formed in the shear band at 77 K. The dislocations inside the grain are evidence of on-going deformation. Fig. 8(a2) shows the break-up of elongated grains in the shear band of UFG 500 nm titanium at 293 K. Recrystallized grain boundaries and triple points are observed in Fig. 8(b2) in the shear band at 173 K; the grains have narrow and faceted boundaries, which are characteristic of recrystallization [61]. Fig. 8(a3) shows the formation of both nano-bundles and recrystallized equiaxed grains in the shear band of UFG 100 nm titanium with initial deformation at 293 K. The dark-field image of the shear band in Fig. 8(b3) demonstrates the formation of nanosized grains inside the shear band at 77 K.

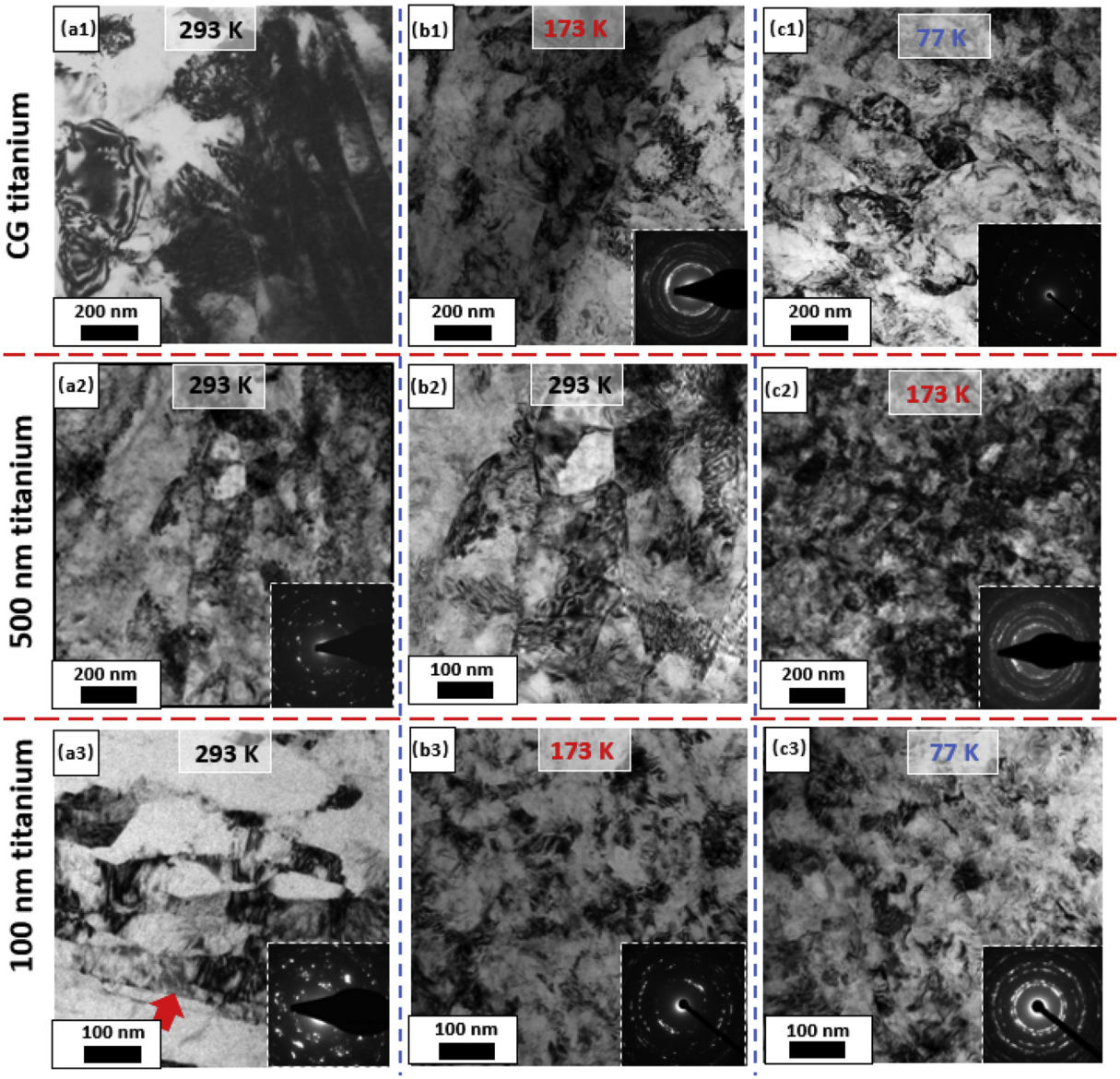

Fig. 7. TEM images of the shear bands formed in CG titanium at (a1) 293 K [9], (b1) 173 K, (c1) 77 K. TEM images of the shear band formed in UFG 500 nm titanium at (a2) 293 K, (b2) 293 K, (c2) 173 K. TEM images of the shear band formed in UFG 100 nm titanium at (a3) 293 K [27], (b3) 173 K, (c3) 77 K.

The grain size distribution inside the shear bands for the different materials and initial deformation temperatures is depicted in Fig. 9. There are clearly two trends: (1) as the initial grain size is decreased, so it is the recrystallized grain size in the shear band; (2) as the initial deformation temperature is decreased, so is the grain size in the shear band.

3.4. Dislocation-based modeling of microstructure evolution inside shear bands

A model that is realistic has to predict the effects of initial deformation temperature and grain size on the nano/microstructure within the shear band. The observations in the previous sections are summarized in Fig. 10. The width of shear band decreases with initial grain size as shown in Fig. 10(a). The recrystallized grain size decreases with the width of shear band as shown in Fig. 10(b).

The local shear strain γ_{local} inside the shear bands was estimated as follows:

$$d_{total} = d_{uniform}\gamma_{uniform} + \delta_{local}\gamma_{local} \tag{7}$$

where d_{total} is the displacement in specimen, δ_{lcoal} is the width of the shear band, and γ is the shear strain. The calculated local shear strains for different shear bands are plotted against the recrystallized grain size in Fig. 10(c). Under the same displacement of hat-shaped specimens, the decrease in the width of the shear band (at cryogenic temperatures) leads to a much larger local shear strain inside the shear bands, which in turn is responsible for the formation of a smaller recrystallized grain size. These are first-order estimates and the local shear strain may be smaller than the calculated ones. However, it is clear that the recrystallized grain size decreases with increasing shear strain inside the band.

The existing rotational recrystallization theory [10,11] does not have this level of detail and therefore needs to be amplified. The evolution of dislocation density with plastic deformation is the result of the combined effects of dislocation generation and annihilation [68]:

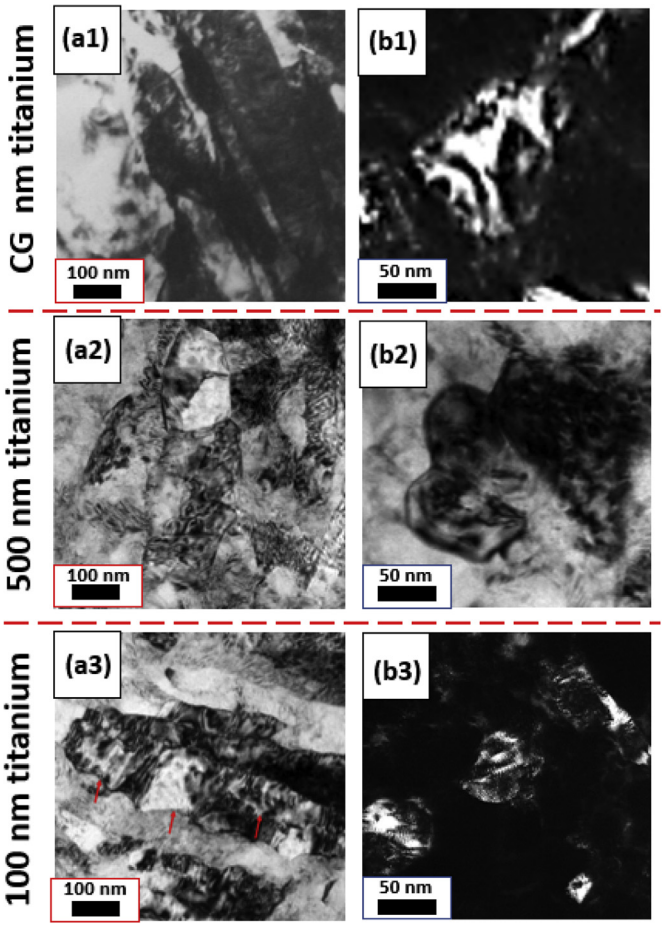

Fig. 8. Microstructure inside the shear bands for CG Ti at (a1) 293 K [9] and (b1) 77 K. Microstructure inside the shear bands for UFG 500 nm Ti at (a2) 293 K and (b2) 173 K. (a3) Microstructure inside the shear bands for UFG 100 nm Ti at 293 K. The red arrows show the formation of recrystallized subgrains in the elongated nano-bundle. (b3) Dark-field image shows the formation of equiaxed subgrains in shear band at 77 K. (For interpretation of the references to colour in this figure legend, the reader is referred to the Web version of this article.)

$$\dot{\rho} = \dot{\rho}_{gen} - \dot{\rho}_{ann} \tag{8}$$

where $\dot{\rho}_{gen}$ and $\dot{\rho}_{ann}$ represent dislocation generation and annihilation rates, respectively.

Kocks and Mecking [69] proposed that the evolution of the dislocation density during plastic deformation is due to the competition between cutting forest dislocations and dynamic recovery of dislocations, and obtained the following expression:

$$\frac{d\rho}{d\gamma} = k_h\sqrt{\rho} - f_s\rho \tag{9}$$

where k_h is a hardening factor and f_s is a softening parameter. The cutting of forest dislocations leads to strain hardening and the annihilation of dislocations by dynamic recovery results in strain softening. Thus, it is possible to estimate the dislocation density at the recrystallization temperature (~0.4 T_m), often considered as required for shear localization.

The energy of randomly distributed dislocations is [10,11]:

$$E_1 = \rho_d\left(\frac{\varpi Gb^2}{4\pi}\right)\ln\left(\frac{\alpha_0}{2b\rho_d^{1/2}}\right) \tag{10}$$

where ϖ is the constant depending on the character of the dislocation, G is the shear modulus, b is Burgers vector, α_0 is a constant which accounts the core energy of the dislocation, and ρ is the dislocation density, which can be estimated throughout the plastic deformation process from the Kocks-Mecking Eqn. (9).

The energy of low-angle grain boundary arrays with the same dislocation density, arranged in ellipsoidal subgrains is:

$$E_2 = \rho_d\left(\frac{\varpi Gb^2}{4\pi}\right)\ln\left[\frac{e\alpha}{4\pi b}\left(\frac{S}{V}\right)\frac{1}{\rho_d}\right] \tag{11}$$

where S and V are surface area and volume of ellipsoid. The ellipsoid has a width W with aspect ratio k. The surface area S and volume V in equation (11) are given by the standard equations [70]:

$$S = 2\pi f(k)(W/2)^2 \tag{12}$$

$$V = \frac{4}{3}\pi k(W/2)^3, \tag{13}$$

$$f(k) = 1 + \frac{k^2}{\sqrt{k^2-1}}\sin^{-1}\left(\frac{\sqrt{k^2-1}}{k}\right) \tag{14}$$

By setting $E_1 = E_2$ in Eqns. (10) and (11), one can obtain the critical dislocation density for dynamic recrystallization:

$$\rho_d^* = \left[\frac{3e}{4\pi}\left(\frac{f(k)}{k}\right)\left(\frac{1}{W/2}\right)\right]^2 \tag{15}$$

It is assumed that when $k \to +\infty$ and $f(k)/k = \pi/2$, the subgrains are the longest and E_1 reaches a maximum. This leads to the following expression:

$$\rho_d^* = \left[\frac{3e}{4}\left(\frac{1}{W}\right)\right]^2 \tag{16}$$

Thus, one can calculate the width of the ellipsoidal subgrains, W:

$$W = \frac{3e\rho^{-1/2}}{4} \tag{17}$$

The Zener-Hollomon parameter [71], Z, was initially used to describe the relationship between flow stress, strain-rate, and temperature:$\ln Z = \ln\dot{\varepsilon} + \frac{Q}{RT}$. The strain-rate inside the shear band is approximately 10^5 s^{-1}, the activation energy for deformation is 150 kJ, and the temperature rise inside the shear band is assumed to be 500 K, the recrystallization temperature for Ti. Mishra et al. [23], Derby [72], and Li et al. [73] found that the recrystallized grain size is proportional to the value ln Z:

$$d_R(\ln Z)^B = A \tag{18}$$

By incorporating (18) into (17) and assuming the width of the ellipsoid equal to the size of recrystallized grains ($W = d_R$), one can obtain the critical dislocation density for shear localization for titanium:

$$\rho_c = \left[\frac{3e}{4}\left(\frac{(\ln Z)^B}{A}\right)\right]^2 \tag{19}$$

where the fitting parameters A and B for CG and UFG 500 nm

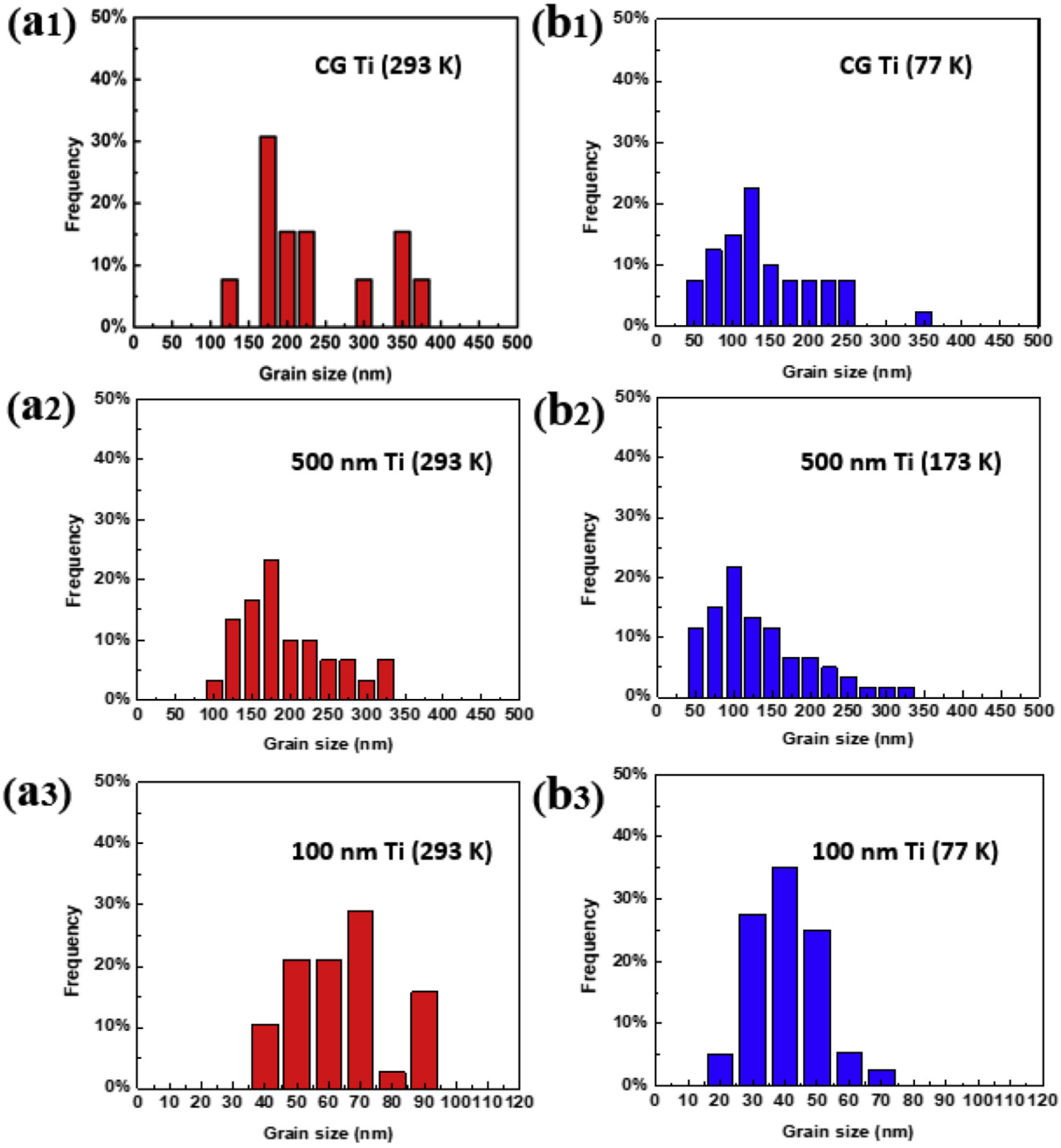

Fig. 9. Grain-size distribution in shear bands in CG titanium at (a1) 293 K and (b1) 77K. Grain-size distribution in shear bands in UFG 500 nm titanium at (a2) 293 K and (b2) 173 K. Grain-size distribution in shear bands in UFG 100 nm titanium at (a3) 293 K and (b3) 77 K.

titanium are summarized in Table 2. These parameters also incorporate the effect of shear strain which can, at some point, be separated into another component. Fig. 11(b1,b2) show the predicted recrystallized grain size d_R and the critical dislocation density for shear localization for CG and UFG 500 nm titanium under different (ln Z) values. Once the critical dislocation density is established, by assuming the initial dislocation density of $6^{*}10^{12}$ m^{-2}, one can obtain the parameters k_h and f_s through the classic Taylor equation [74] ($\tau = \tau_0 + \alpha_0 Gb\sqrt{\rho}$, where τ_0 is the yield shear stress, α_0 is a constant taken as 0.09, $G = 45$ GPa is the shear modulus, and b is the Burgers vector taken as 0.289 nm). Table 3 shows other parameters for the Kocks-Mecking theory. It can be seen that the critical dislocation density increases with decreasing grain size, leading to a decrease in W (as predicted from Eqn. (17)) and a consequent decrease in recrystallized grain size. The same trend is observed for the decrease in initial deformation temperature. Fig. 11 (a1,a2) show that the rate of change of dislocation density first increases and then decreases gradually to zero.

Once the subgrain configuration forms (with a width W), it tends to break into segments which rotate to accommodate further deformation. Meyers et al. [9] showed that the recrystallized grain size of CG titanium inside the shear band could not reach the nanocrystalline region assuming static migrational recrystallization during the cooling of the shear band, thus demonstrating that the migrational recrystallization mechanism cannot account for the formation of recrystallized grains inside the shear band.

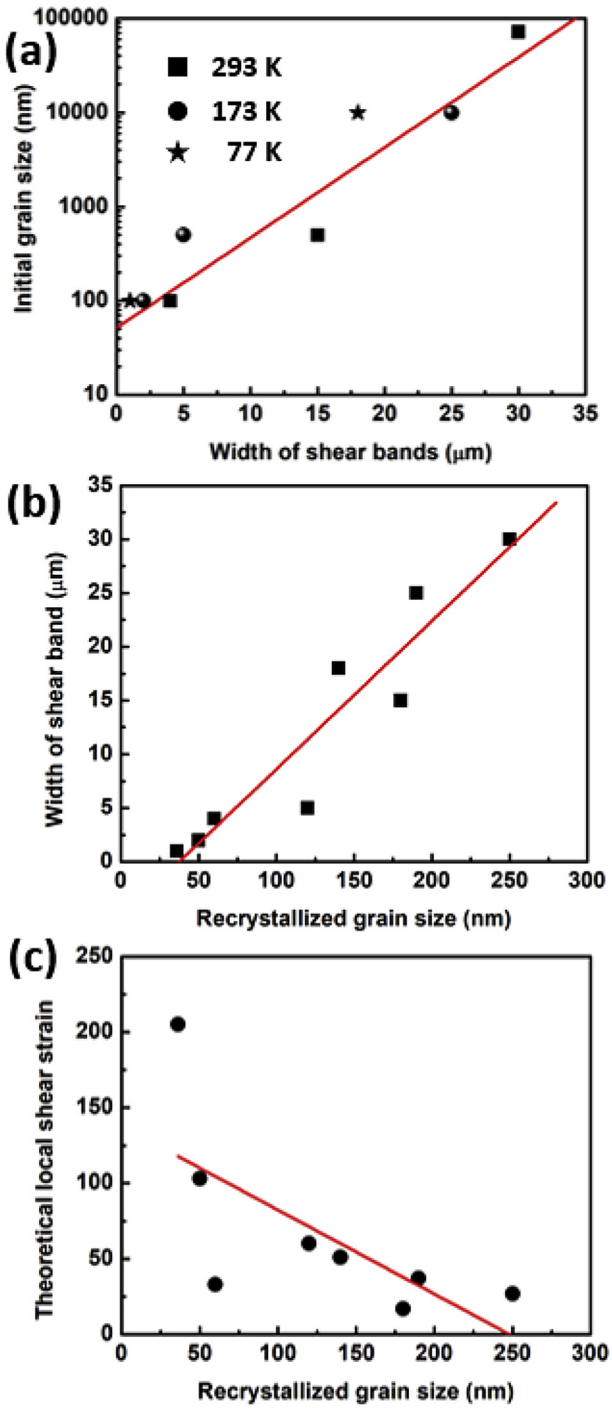

Fig. 10. (a) Width of shear band as a function of initial grain size. (b) Recrystallized grain size as a function of shear band width. (c) Recrystallized grain size as a function of estimated local shear strain.

Table 2
Parameters for the relationship of Zener-Hollomon parameter [71] with the average recrystallized grain size for titanium.

	A	B
CG Ti	1.51*10^6	2.47
UFG 500 nm Ti	6.96*10^7	3.65

Thus, Meyers et al. [9–11], and Hines and Vecchio et al. [60] proposed that a rotational dynamic recrystallization had to occur to account for the observed grain size refinement inside the shear band. As calculated using Eqn. (2), the temperature inside the shear bands can rise to the recrystallization temperature (between 0.4 T_m–0.5 T_m) for both CG and UFG titanium. Once the elongated subgrains are achieved, they further break up into subgrains. According to the rotational dynamic recrystallization mechanism, the formation of a new equiaxed grain requires a final step: local grain-boundary segments to tilt about 30° within the deformation process [11]. The time needed for these processes can be expressed as follows [11]:

$$t = \frac{WkTf(\theta)}{4\delta_g \eta D_{b0} \exp(-Q_b/RT)} \tag{20}$$

where t is time; W is the average grain diameter ($=d_R$); δ_g is grain-boundary thickness; η is the grain-boundary energy; D_{b0} is a constant related to grain boundary diffusion; Q_b is the activation energy for grain boundary diffusion; θ is the subgrain misorientation. $f(\theta)$ is given in Ref. [11]:

$$f(\theta) = \frac{3\tan(\theta) - 2\cos(\theta)}{3 - 6\sin(\theta)} + \frac{2}{3} - \frac{4\sqrt{3}}{9}\ln\frac{2+\sqrt{3}}{2-\sqrt{3}} + \frac{4\sqrt{3}}{9}\ln\frac{\tan(\theta/2) - 2 - \sqrt{3}}{\tan(\theta/2) - 2 + \sqrt{3}} \tag{21}$$

For UFG titanium, $\delta_g = 1.5 \times 10^{-9}$ m, $\eta = 0.675$ J/m^2, $D_{b0} = 1.4 \times 10^{-3}$ m^2/s, $Q_b = 151$ kJ/mol, $k = 1.38 \times 10^{-23}$ J/K, $R = 8.314$ J/(K·mol), and $T = 800$ K [9,27]. The kinetic curves for the rotational dynamic recrystallization mechanism in a shear band can be obtained by integrating the parameters in Equations (20) and (21). Fig. 12 shows that a grain boundary can rotate 30° within 6 μs for a grain size of 200 nm; for a grain size of 40 nm, the time is reduced to 2 μs since the diffusion path is shortened. The total deformation time in the hat-shaped specimen is ~200 μs. Thus, there is ample time for the boundary segments to reorient to minimize their energy and create an equiaxed configuration during deformation. The schematic drawing showing the dynamic recrystallization process of UFG 100 nm is presented in Fig. 13(a–c). With the increase of shear deformation, the initial grain size breaks down into smaller domains. Once the low-angle grain boundaries form, the grains tend to rotate by θ to form equiaxed grains due to energy gradients.

3.5. Cooling of the shear bands

It is important to establish the cooling times for the shear bands with different thickness. Assuming a constant rate of heat generation in the thin shearing zone, the solution of the heat equation for the hat-shaped specimens can be reduced to [75]:

$$T(x,t) = \frac{\delta(T_m - T_0)}{\sqrt{4\pi\chi t}} e^{-(x-R_i)^2/4\chi t} \left(R_i - \frac{\delta}{2} < x < R_i + \frac{\delta}{2}\right) \tag{22}$$

where T_0 and T_m are the initial temperature and the maximum temperature within the shear band after the deformation; t, δ and R_i are the cooling time, the width of shear bands and the distance from the center of shear band to the center of the hat-shaped specimen; χ is the heat diffusivity. $\Delta T = T_m - T_0 = 500$ K is assumed for each shear band and x is equal to R_i in the middle of shear band. The fast cooling rates of shear bands at room and low temperatures shown in Fig. 14 are responsible for retaining the ultrafine- and nano-grain size inside the shear band and not

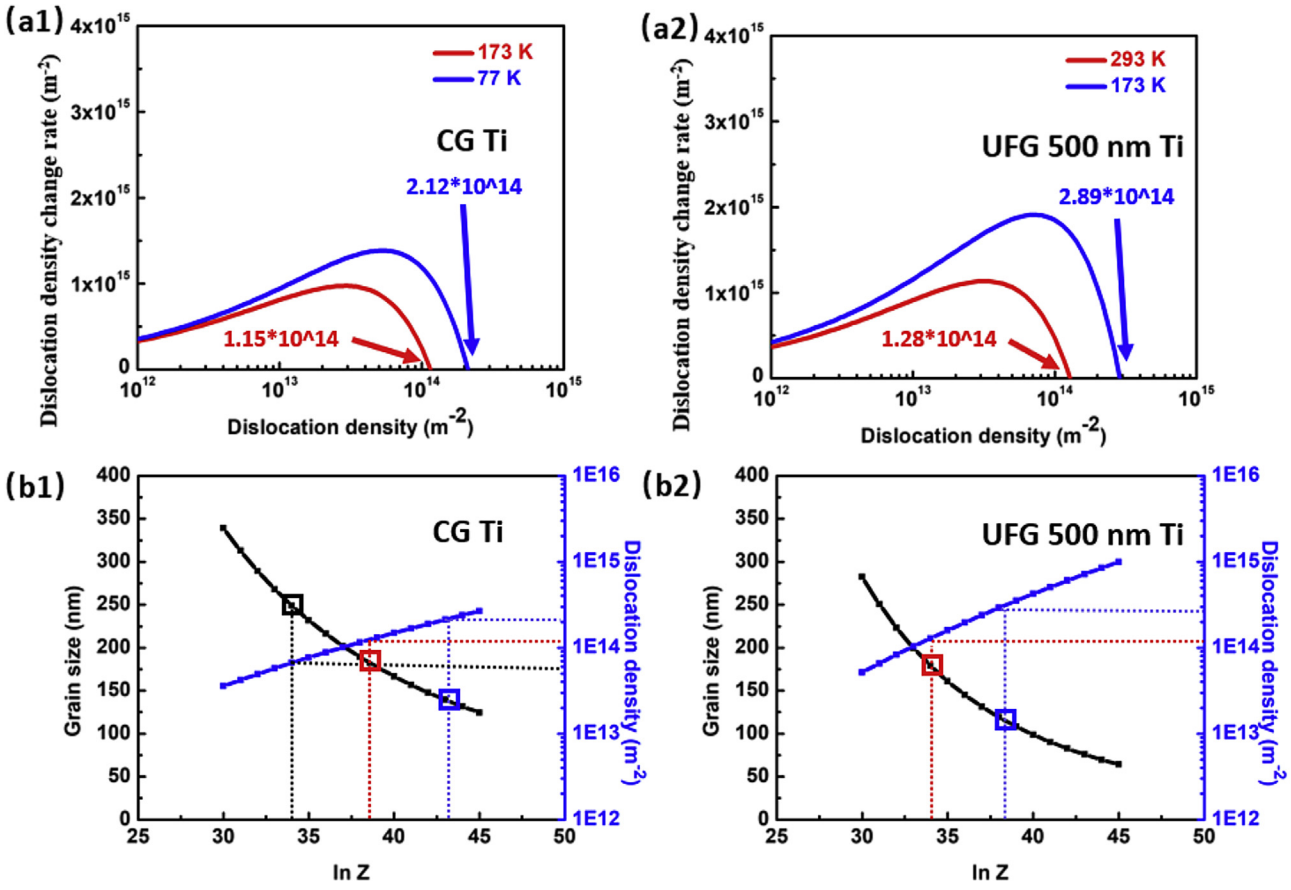

Fig. 11. (a1,a2) Rate of dislocation density change with the variation of dislocation density. (b1,b2) Relationship between critical dislocation density and subgrain size with Zener-Hollomon parameter (ln Z).

Table 3
Constants for the Kocks-Mecking model [69] and critical dislocation densities for shear localization.

Parameters	k_{forest}	$f_{recovery}$	Critical dislocation density (m^{-2})
CG Ti (173 K)	3.63*10^8	33.8	1.15*10^14
CG Ti (77 K)	3.81*10^8	26.2	2.12*10^14
500 nm Ti (293 K)	4.01*10^8	35.4	1.28*10^14
500 nm Ti (173 K)	4.50*10^8	26.5	2.89*10^14

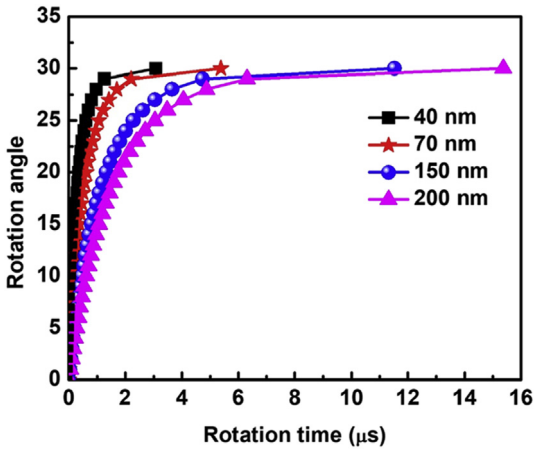

Fig. 12. Rotation of grain-boundary segments as a function of time at 800 K for grain sizes of 40 nm, 70 nm, 150 nm and 200 nm.

allowing the grains to grow during cooling. Although there are differences among the different initial conditions, the cooling to ambient temperature occurs within 20 μs for most specimens. These calculations confirm that the grains inside the shear band are formed by the rotational dynamic recrystallization process, and not by static migrational recrystallization during cooling.

4. Conclusions

Taken as a whole, the mechanical behavior and adiabatic shear band formation of CG and UFG titanium at room and cryogenic temperatures were revealed and several new findings were made which can be summarized as follows:

(1) The strength of UFG titanium is significantly higher compared with CG titanium due to the Hall-Petch effect. In comparison with CG titanium, the strain hardening rate of the UFG titanium is significantly lower due to the reduced dislocation activation volume and larger incidence of grain boundaries which act as dislocation sinks. The strain-rate sensitivity of UFG titanium does not change significantly with temperature, in comparison with CG titanium, indicating no significant change of deformation mechanism.
(2) The width of the shear band of CG titanium does not change too much with decreasing temperature. In contrast, the width of shear band of UFG 500 nm titanium decreases from ~15 μm formed at room temperature to ~5 μm at low temperature. The width of shear band of UFG 100 nm titanium decreases to ~1 μm at low temperature, which is one quarter

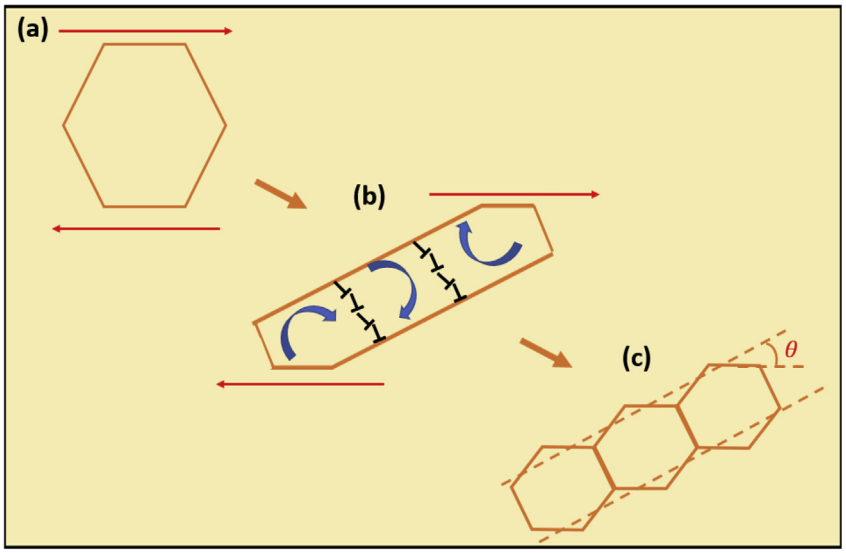

Fig. 13. Schematic drawing showing the shear-rotational dynamic recrystallization mechanism for UFG 100 nm to form recrystallized equiaxed nanograins. (a) Original ultrafine-grains; (b) formation of low-angle grain boundaries and subsequent grain rotation under the applied shear stress; (c) formation of recrystallized equiaxed nanograins through grain-boundary rotation by an angle θ.

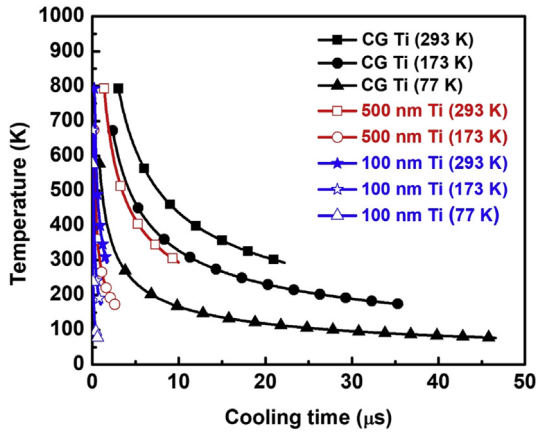

Fig. 14. Temperature in the middle of the shear bands as a function of cooling time for CG and UFG titanium [75].

of that (~4 μm) formed at room temperature. The combined effects of the decrease of thermal conductivity, the decrease of specific heat capacity and the increase of thermal softening for UFG titanium lead to decreased widths according to Bai-Dodd's and Grady's predictions and are indeed experimentally observed. The experimental results fall within the region bound by the two theories and show a strength sensitivity slightly higher than them; the values are closer to the Bai-Dodd theory for lower strength levels (CG) and approach the Grady theory for higher strength (UFG) Ti.

(3) A dislocation-based Kocks-Mecking model is proposed to describe the dislocation evolution prior to the dynamic recrystallization process for CG and UFG 500 nm titanium. The dislocation density increases gradually until it reaches the critical value determined by a balance in dislocation generation and annihilation. The randomly distributed dislocations form elongated ellipsoid configurations which, once the temperature reaches the recrystallization value (~0.4 $T_{melting}$), break down through subgrain rotation. It is shown that the width of the sub-grains decreases with increasing dislocation density.

(4) The formation of nanograins inside the shear bands is explained in terms of the rotational dynamic recrystallization mechanism, which is expanded to incorporate the differences observed for the different initial conditions (grain size, initial deformation temperature, and shear strain).

(5) A reduction in the recrystallized grain size inside the shear bands for both CG and UFG titanium is observed for the initial deformation temperature in the cryogenic region. This is caused by a higher dislocation density reached at the onset of recrystallization due to higher accumulation rates in the first stage of deformation, at sub-ambient temperatures.

(6) The Zener-Hollomon parameter was used to predict the recrystallized grain size and critical dislocation density for shear localization. Additionally, the larger local shear strain in the shear bands at cryogenic temperatures, because of the decrease of width, also contributes to a more severe plastic deformation, inducing smaller grain size inside the shear band.

Acknowledgements

This work was supported by the U.S. Department of Energy through grant NNSA/SSAP (DE-NA0002080) and the UCSD Center for High Energy Density Science (UCOP LAB FEES GRANT ID: LFR-17-449059) (for M.A.M.). Support of Zezhou Li by China Scholarship Council (201508020004) is also greatly acknowledged. RZV gratefully acknowledges the financial support from Russian Science Foundation (project No. 19-49-02003). Partial support for MAM from the NNSA/DOE (DE-NA0003842)Center for Matter under Extreme Pressure Conditions (CMEC) is also gratefully acknowledged.

References

[1] Y. Me-Bar, D. Shechtman, On the adiabatic shear of Ti-6Al-4V ballistic targets, Mater. Sci. Eng. 58 (1983) 181–188.
[2] S.P. Timothy, I.M. Hutchings, The structure of adiabatic shear bands in a titanium alloy, Acta Metall. 33 (1985) 667–676.
[3] H.A. Grebe, H.-r. Pak, M.A. Meyers, Adiabatic shear localization in titanium and Ti-6 Pct Al-4 Pct V alloy, Metall. Trans. A 16 (5) (1985) 761–775.
[4] M.A. Meyers, H.-r. Pak, Observation of an adiabatic shear band in titanium by high-voltage transmission electron microscopy, Acta Metall. 34 (1986)

2493–2499.
[5] S.P. Timothy, The structure of adiabatic shear bands in metals: a critical review, Acta Metall. 35 (1987) 301–306.
[6] R.E. Winter, Adiabatic shear in titanium and polymethylmethacrylate, Philos. Mag. 31 (1974) 765–773.
[7] R.Z. Valiev, T.G. Langdon, Principles of equal-channel angular pressing as a processing tool for grain refinement, Prog. Mater. Sci. 51 (2006) 881–981.
[8] D. Banerjee, J.C. Williams, Perspectives on titanium science and technology, Acta Mater. 61 (2013) 844–879.
[9] M.A. Meyers, G. Subhash, B.K. Kad, L. Prasad, Evolution of microstructure and shear band formation in α-hcp titanium, Mech. Mater. 17 (1994) 175–193.
[10] M.A. Meyers, J.C. LaSalvia, V.F. Nesterenko, Y.J. Chen, B.K. Kad, in: T.R. McNelley (Ed.), Dynamic Recrystallization in High Strain Rate Deformation, Recrystallization and Related Phenomena, Rex'96, Monterey, 1997, pp. 279–286.
[11] M.A. Meyers, V.F. Nesterenko, J.C. LaSalvia, Q. Xue, Shear localization in dynamic deformation of materials: microstructural evolution and self-organization, Mater. Sci. Eng. A 317 (2001) 204–225.
[12] B. Dodd, Y. Bai (Eds.), Adiabatic Shear Localization: Frontiers and Advances, Elsevier, 2012.
[13] R.Z. Valiev, Materials science: nanomaterial advantage, Nature 419 (6910) (2002) 887.
[14] R.Z. Valiev, Nanostructuring of metals by severe plastic deformation for advanced properties, Nat. Mater. 3 (8) (2004) 511.
[15] L. Lu, X. Chen, X. Huang, K. Lu, Revealing the maximum strength in nanotwinned copper, Science 323 (2009) 607–610.
[16] X. Li, K. Lu, Playing with defects in metals, Nat. Mater. 16 (7) (2017) 700.
[17] M.A. Meyers, A. Mishra, D.J. Benson, Mechanical properties of nanocrystalline materials, Prog. Mater. Sci. 51 (2006) 427–556.
[18] H. Gleiter, Nanostructured materials: basic concepts and microstructure, Acta Mater. 48 (1) (2000) 1–29.
[19] M.A. Meyers, E. Ashworth, A model for the effect of grain size on the yield stress of metals, Philos. Mag. A 46 (1982) 737–759.
[20] H. Van Swygenhoven, P.M. Derlet, A.G. Frøseth, Nucleation and propagation of dislocations in nanocrystalline fcc metals, Acta Mater. 54 (2006) 1975–1983.
[21] H. Conrad, J. Narayan, On the grain size softening in nanocrystalline materials, Scr. Mater. 42 (2000) 1025–1030.
[22] A.J. Haslam, D. Moldovan, S.R. Phillpot, D. Wolf, H. Gleiter, Combined atomistic and mesoscale simulation of grain growth in nanocrystalline thin films, Comput. Mater. Sci. 23 (2002) 15–32.
[23] A. Mishra, M. Martin, N.N. Thadhani, B.K. Kad, E.A. Kenik, M.A. Meyers, High-strain-rate response of ultra-fine-grained copper, Acta Mater. 56 (2008) 2770–2783.
[24] B.K. Kad, J.-M. Gebert, M.T. Pérez-Prado, M.E. Kassner, M.A. Meyers, Ultrafine-grain-sized zirconium by dynamic deformation, Acta Mater. 54 (2006) 4111–4127.
[25] D. Jia, Y.M. Wang, K.T. Ramesh, E. Ma, Y.T. Zhu, R.Z. Valiev, Deformation behavior and plastic instabilities of ultrafine-grained titanium, Appl. Phys. Lett. 79 (2001) 611–613.
[26] D. Jia, K.T. Ramesh, E. Ma, Failure mode and dynamic behavior of nanophase iron under compression, Scr. Mater. 42 (2000) 73–78.
[27] Z. Li, B. Wang, S. Zhao, R.Z. Valiev, K.S. Vecchio, M.A. Meyers, Dynamic deformation and failure of ultrafine-grained titanium, Acta Mater. 125 (2017) 210–218.
[28] Y.-J. Chen, M.A. Meyers, V.F. Nesterenko, Spontaneous and forced shear localization in high-strain-rate deformation of tantalum, Mater. Sci. Eng. A 268 (1999) 70–82.
[29] D.V. Gunderov, A.V. Polyakov, I.P. Semenova, G.I. Raab, A.A. Churakova, E.I. Gimaltdinova, I. Sabirov, J. Segurado, V.D. Sitdikov, I.V. Alexandrov, N.A. Enikeev, R.Z. Valiev, Evolution of microstructure, macrotexture and mechanical properties of commercially pure Ti during ECAP-conform processing and drawing, Mater. Sci. Eng. A 562 (2013) 128–136.
[30] G.S. Dyakonov, S. Mironov, I.P. Semenova, R.Z. Valiev, S.L. Semiatin, Microstructure evolution and strengthening mechanisms in commercial-purity titanium subjected to equal-channel angular pressing, Mater. Sci. Eng. A 701 (2017) 289–301.
[31] G.S. Dyakonov, S. Mironov, N. Enikeev, I.P. Semenova, R.Z. Valiev, S.L. Semiatin, Annealing behavior of severely-deformed titanium Grade 4, Mater. Sci. Eng. A 742 (2019) 89–101.
[32] G.S. Dyakonov, S. Mironov, I.P. Semenova, R.Z. Valiev, S.L. Semiatin, EBSD analysis of grain-refinement mechanisms operating during equal-channel angular pressing of commercial-purity titanium, Acta Mater. 173 (2019) 174–183.
[33] L.J. van der Pauw, A method of measuring specific resistivity and Hall effect of discs of arbitrary shape, Philips Res. Rep. 13 (1958) 1–9.
[34] L.J. van der Pauw, A method of measuring the resistivity and hall coefficient on lamellae of arbitrary shape, Philips Res. Rep. 20 (1959) 220–224.
[35] R. Franz, G. Wiedemann, Ueber die Wärme-Leitungsfähigkeit der Metalle, Ann. Phys. 165 (8) (1853) 497–531.
[36] R.W. Powell, R.P. Tye, The thermal and electrical conductivity of titanium and its alloys, J. Less Comm. Met. 3 (1961) 226–233.
[37] A.V. Sergueeva, V.V. Stolyarov, R.Z. Valiev, A.K. Mukherjee, Advanced mechanical properties of pure titanium with ultrafine grained structure, Scr. Mater. 45 (2001) 747–752.
[38] R.W. Armstrong, 60 years of Hall-Petch: past to present nano-scale connections, Mater. Trans. 55 (1) (2014) 2–12.
[39] F.W. Long, Q.W. Jiang, L. Xiao, X.W. Li, Compressive deformation behaviors of coarse-and ultrafine-grained pure titanium at different temperatures: a comparative study, Mater. Trans. 52 (8) (2011) 1617–1622.
[40] D. Jia, K.T. Ramesh, E. Ma, Effects of nanocrystalline and ultrafine grain sizes on constitutive behavior and shear bands in iron, Acta Mater. 51 (2003) 3495–3509.
[41] Y.G. Ko, D.H. Shin, K.-T. Park, C.S. Lee, An analysis of the strain hardening behavior of ultra-fine grain pure titanium, Scr. Mater. 54 (2006) 1785–1789.
[42] V.Z. Bengus, E.D. Tabachnikova, V.D. Natsik, Ĭ. Mishkuf, K. Chakh, V.V. Stolyarov, R.Z. Valiev, Low-temperature deformation and fracture of bulk nanostructural titanium obtained by intense plastic deformation using equal channel angular pressing, Low Temp. Phys. 28 (2002) 864.
[43] S. Nemat-Nasser, W.G. Guo, J.Y. Cheng, Mechanical properties and deformation mechanisms of a commercially pure titanium, Acta Mater. 47 (1999) 3705–3720.
[44] D.R. Chichili, K.T. Ramesh, K.J. Hemker, The high-strain-rate response of alpha-titanium: experiments, deformation mechanisms and modeling, Acta Mater. 46 (1998) 1025–1043.
[45] R.S. Culver, Metallurgical Effects at High Strain Rates, Plenum Press, 1973.
[46] M.A. Meyers, Dynamic Behavior of Materials, Wiley, 1994.
[47] Y. Guo, Q. Ruan, S. Zhu, Q. Wei, H. Chen, J. Lu, B. Hu, X. Wu, Y. Li, D. Fang, Temperature rise associated with adiabatic shear band: causality clarified, Phys. Rev. Lett. 122 (1) (2019), 015503.
[48] Q. Xue, M.A. Meyers, V.F. Nesterenko, Self-organization of shear bands in titanium and Ti–6Al–4V alloy, Acta Mater. 50 (2002) 575–596.
[49] B. Dodd, Y.L. Bai, Width of adiabatic shear bands found under combined stress, Mater. Sci. Technol. 5 (1989) 557–559.
[50] D.E. Grady, Dissipation in adiabatic shear bands, Mech. Mater. 17 (1994) 289.
[51] D.E. Grady, in: TMS Symposium on Dynamic Behavior of Materials, 2007. Warrendale, PA.
[52] F.A. Guo, K.Y. Zhu, N. Trannoy, J. Lu, Examination of thermal properties by scanning thermal microscopy in ultrafine-grained pure titanium surface layer produced by surface mechanical attrition treatment, Thermochim. Acta 419 (2004) 239–246.
[53] P. Debye, Zur Theorie der spezifischen Wärmen, Ann. Phys. 344 (1912) 789–839.
[54] D.R. Gaskell, Introduction to the Thermodynamics of Materials, Taylor & Francis group, 2008.
[55] K.K. Kelley, Specific heats at low temperatures of titanium and titanium carbide, Ind. Eng. Chem. 36 (1944) 866.
[56] X. Sun, Y. Guo, Q. Wei, Y. Li, S. Zhang, A comparative study on the microstructure and mechanical behavior of titanium: ultrafine grain vs. coarse grain, Mater. Sci. Eng. A 669 (2016) 226–245.
[57] P. Hidnert, Thermal expansion of titanium, J. Res. Natl. Bur. Stand. 30 (1943) 101–105.
[58] S.-C. Liao, J. Duffy, Adiabatic shear bands in a Ti-6Al-4V titanium alloy, J. Mech. Phys. Solids 46 (1998) 2201–2231.
[59] J.A. Hines, K.S. Vecchio, S. Ahzi, A model for microstructure evolution in adiabatic shear bands, Mater. Trans. A 29 (1998) 191–203.
[60] J.A. Hines, K.S. Vecchio, Recrystallization kinetics within adiabatic shear bands, Acta Metall. 45 (1997) 635–649.
[61] U. Andrade, M.A. Meyers, K.S. Vecchio, A.H. Chokshi, Dynamic recrystallization in high-strain, high-strain-rate plastic deformation of copper, Acta Mater. 42 (1994) 3183–3195.
[62] C. Zhu, V. Livescu, T. Harrington, O. Dippo, G.T. Gray III, K.S. Vecchio, Investigation of the shear response and geometrically necessary dislocation densities in shear localization in high-purity titanium, Int. J. Plast. 92 (2017) 148–163.
[63] Q. Wei, L. Kecskes, T. Jiao, K.T. Hartwig, K.T. Ramesh, E. Ma, Adiabatic shear banding in ultrafine-grained Fe processed by severe plastic deformation, Acta Mater. 52 (7) (2004) 1859–1869.
[64] S. Li, N.R. Tao, K. Lu, Microstructural evolution and nanostructure formation in copper during dynamic plastic deformation at cryogenic temperatures, Acta Mater. 56 (2) (2008) 230–241.
[65] J.L. Sun, P.W. Trimby, F.K. Yan, X.Z. Liao, N.R. Tao, J.T. Wang, Grain size effect on deformation twinning propensity in ultrafine-grained hexagonal close-packed titanium, Scr. Mater. 69 (5) (2013) 428–431.
[66] K. Lu, L. Lu, S. Suresh, Strengthening materials by engineering coherent internal boundaries at the nanoscale, Science 324 (2009) 349–352.
[67] F. Yan, H.W. Zhang, N.R. Tao, K. Lu, Quantifying the microstructures of pure Cu subjected to dynamic plastic deformation at cryogenic temperature, J. Mater. Sci. Technol. 27 (2011) 673–679.
[68] M. Bacca, D.R. Hayhurst, R.M. McMeeking, Continuous dynamic recrystallization during severe plastic deformation, Mech. Mater. 90 (2015) 148–156.

[69] U.F. Kocks, H. Mecking, Physics and phenomenology of strain hardening: the FCC case, Prog. Mater. Sci. 48 (2003) 171–273.
[70] J.P. Hirth, J. Lothe, T. Mura, Theory of dislocations, J. Appl. Mech. 50 (1983) 476.
[71] C. Zener, J.H. Hollomon, Effect of strain rate upon plastic flow of steel, J. Appl. Phys. 15 (1) (1944) 22–32.
[72] B. Derby, The dependence of grain size on stress during dynamic recrystallization, Acta Metall. Mater. 39 (1991) 955–962.
[73] Y.S. Li, Y. Zhang, N.R. Tao, K. Lu, Effect of the Zener–Hollomon parameter on the microstructures and mechanical properties of Cu subjected to plastic deformation, Acta Mater. 57 (3) (2009) 761–772.
[74] G.I. Taylor, The mechanism of plastic deformation of crystals, Proc. R. Soc. Lond. 143 (1934) 362–378.
[75] S. Nemat-Nasser, J.B. Isaacs, M. Liu, Microstructure of high-strain, high-strain-rate deformed tantalum, Acta Mater. 46 (1998) 1307–1325.